Effects of implant buccal distance on peri-implant strain: A Micro-CT based finite element analysis

Kangning Su [a], Yuxiao Zhou [a], Mehran Hossaini-Zadeh [b], Jing Du [a,*]

[a] *Department of Mechanical Engineering, Pennsylvania State University, University Park, PA, USA*
[b] *Department of Oral Maxillofacial Pathology Medicine and Surgery, Temple University, Philadelphia, PA, USA*

ARTICLE INFO

ABSTRACT

Bone-implant mechanics is one of the factors that contribute to implant stability and success. In this work, voxel-based finite element models were built based on the micro-CT images of human cadaveric mandible specimens before and after implant placement. The computed results show high strain at the bone-implant contact locations and the buccal and lingual bone plates. The strain concentration in the thinner buccal plates was more substantial than that in the thicker lingual plates. The average values of maximum principal strain in the buccal and lingual ROIs were in good agreement with those measured using mechanical testing coupled with micro-CT and digital volume correlation.

The implant position was then virtually changed in the models to be placed lingually or buccally. The computed strain in the buccal bone decreased when the implant was placed away from the buccal plate. The strain in lingual bone also deceased when the implant was moved from the center of the alveolar socket towards the lingual or buccal plate. The results indicate that the distance from implant to the buccal plate can affect the mechanical stimuli in bone, especially in the buccal plate, which may subsequently affect the bone remodeling process and buccal bone resorption.

1. Introduction

Immediate implant placement is a treatment method to install dental implants immediately after tooth extraction, aiming to preserve the alveolar bone dimensions after tooth loss. One risk of immediate implant placement is buccal (lip-side) bone resorption, of which the mechanisms are still not clear (Chen and Buser, 2009, 2014; Kan et al., 2010). Mechanics of bone-implant complex is one of the factors that contribute to implant stability and success (Brunski, 1992; Leucht et al., 2007; Wazen et al., 2013).

In our prior experimental work, strain in alveolar bone under implant loading was mapped using mechanical testing coupled with micro X-ray computed tomography (micro-CT) and digital volume correlation (Du et al., 2015; Zhou et al., 2020). High strain appeared at bone-implant contact regions, as well as in buccal and lingual (tongue-side) bone plates although these regions were not directly in contact with implants. The strain concentration in the thinner buccal plate was more substantial than that in the thicker lingual plate. In our prior computational work, voxel-based models were built based on the micro-CT images, and the strain in bone under implant loading was computed using finite element method (FEM) (Mao et al., 2019). The computed strain distribution patterns qualitatively agreed with our experimental results.

In this paper, voxel-based finite element models were built based on the micro-CT images of human cadaveric mandible specimens before and after implant placement. The computed strain values in buccal and lingual bone plates were quantitatively compared with those measured by experiments. The implant position was then virtually changed in the models by translating the implant towards the buccal or the lingual direction. The strain in bone with different implant positions was calculated and compared. The effects of implant position on the bone-implant mechanics and bone resorption were discussed.

2. Materials and methods

2.1. Sample preparation and mechanical testing coupled with micro-CT imaging

This study was exempted by Institutional Review Board (IRB) at the Pennsylvania State University (STUDY00007794). Two fresh-frozen

---

* Corresponding author. Department of Mechanical Engineering 316B Leonhard Building University Park, PA, 16802, USA.
E-mail addresses: kxs535@psu.edu (K. Su), yyz5239@psu.edu (Y. Zhou), mhossaini@temple.edu (M. Hossaini-Zadeh), jingdu@psu.edu (J. Du).

human cadaveric mandibles were obtained from National Disease Research Interchange (NDRI). The mandibles were sectioned to specimens, each containing a bicuspid (#29 in the universal numbering system) and two adjacent teeth. Micro-CT scans (Phoenix v|tome|x L300, GE, Boston, MA) were performed to obtain bone-tooth images with an isometric voxel size of 15 μm. The teeth #29 were then extracted and replaced by dental implants (SLActive® Roxolid®, TiZr, Straumann, Basel, Switzerland) by a practicing dentist.

Mechanical testing was performed on the bone-implant specimens using a loading device (CT5000, Deben, Suffolk, UK) coupled with micro-CT. A compressive load was applied on the implants quasi-statically until it reached 100 N. Micro-CT scans were performed before loading and after 1-hr holding, respectively. 3D full-field strain inside the bone was calculated by digital volume correlation (DVC) using DaVis software (LaVision, Goettingen, Germany). The detailed protocols for the experiments can be found in our prior publications (Du et al., 2015; Zhou et al., 2020).

2.2. Finite element modeling

The micro-CT images were segmented into bone, implant, teeth and background, using Avizo software (FEI Visualization Sciences Group, Burlington, MA). The void spaces among trabecular bone were included in the label of bone. In the bone-tooth images, teeth #29 were virtually removed and replaced by implants segmented from the bone-implant images. The modified micro-CT images were converted to voxel-based 3-dimensional (3D) finite element models by our custom-written MATLAB code (MathWorks, Inc., Natick, MA). Schematics of one representative model (specimen #1) is presented in Fig. 1. The teeth and implants were assumed to be fully bonded to bone. The periodontal ligaments were neglected. Adjacent voxels were combined to form linear hexahedral elements with an isometric size of 90 μm. Each model contained ~5 million elements. The models were then imported into Abaqus (Dassault Systèmes Simulia Corporation, Providence, RI).

All materials were assumed to be linear elastic and isotropic. The Poisson's ratios were chosen to be 0.3, 0.31 and 0.34 for bone, tooth and implant, respectively. The Young's modulus of implants was chosen to be 110 GPa (Brizuela-Velasco et al., 2017; Mao et al., 2019; Soboyejo, 2003). For simplicity, Young's modulus of dentin, 15.0 GPa, was used for the whole teeth (Mao et al., 2019). The Young's modulus of each bone element was assigned using our custom-written Python code. It was given by:

$$E = C \cdot I^2 \tag{1}$$

where E is Young's modulus and I is the average intensity of all voxels in this bone element. The constant C was adjusted to minimize the difference in the strain values obtained from simulation and experiments, detailed in Section 2.3. The elements with Young's modulus less than 0.432 GPa was considered to be the void spaces among trabecular bone. These elements were also assigned with moduli based on equation (1) and included in the simulations, but were not displayed in the figures.

Boundary conditions and loads were applied in the models to mimic the loading conditions in the experiments (Mao et al., 2019). The bottom part of the models (blue and orange in Fig. 1) was fully fixed. A static load of 100 N along the vertical axis of the specimen was uniformly distributed on the top surface of the implant (Fig. 1). Finite element simulations were carried out in Abaqus to compute the strain in bone under implant loading.

2.3. Comparison with experiments

The method of comparing strains in regions of interest (ROI) at the vicinity of implant was adopted from prior work by Korabi et al. (2017). Two ROIs were defined at the buccal and lingual side of the bone surrounding the upper part of implants, respectively (Fig. 1). In simulation results, the maximum principal strain in bone elements in each ROI, including the void spaces among trabecular bone, was extracted. In experimental results, the maximum principal strain in all correlation windows in each ROI was also extracted. The average and standard deviation were calculated, respectively. The computed average strain in each ROI was compared with the experimentally measured strain.

2.4. Implant buccal distance

In each model, the implant was virtually translated towards the buccal or the lingual direction in the micro-CT images using Avizo (Fig. 2). The bone-implant contact areas were also calculated using Avizo (Du et al., 2015). To compare between specimens with different morphologies, relative buccal distance of the implant was used. It is given by
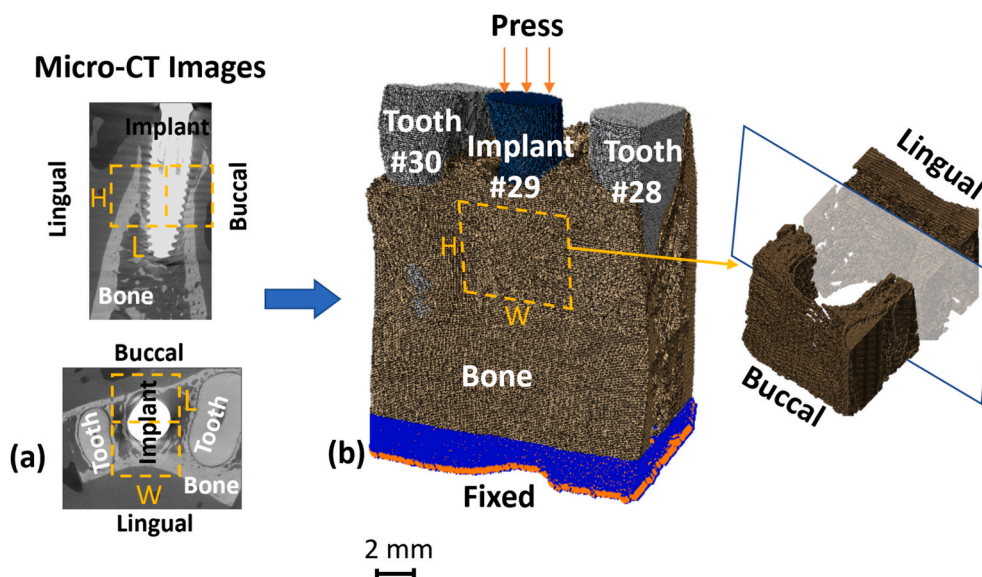

Fig. 1. (a) Micro-CT images of a representative bone-implant specimen #1; (b)Voxel-based finite element model of this specimen. Inset image showing the buccal and lingual ROIs. Dimensions of the ROIs: Hight (H) – 5.25 mm, Width (W) – 7.37 mm, Length (L) – 5.5 mm.
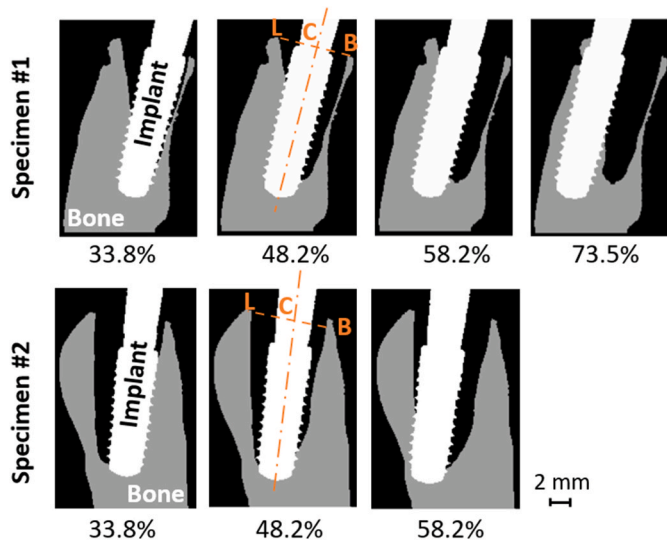
Fig. 2. Buccal-lingual sections of the finite element models with different relative buccal distance (CB/LB) for implant. B – buccal crest; L-lingual crest; C – center of implant.

$$\delta_b = \frac{CB}{LB} \times 100\% \qquad (2)$$

where CB is the distance from the center of the implant to the buccal crest and LB is the distance from the lingual crest to the buccal crest in the sagittal section going through the center of implants (Fig. 2). Hence, 100% refers to the buccal crest and 0% refers to the lingual crest. In the experiments, the buccal distances for the two specimens were both 48.2%.

FEM models were built using the methods in section 2.2 with the same material properties, load and boundary conditions. Strain in bone under implant loading in these models was calculated by FEM in Abaqus. Average strain in the same ROIs defined in section 2.3 was calculated.

3. Results

3.1. Strain in peri-implant bone

The constant C in Equation (1) was chosen to be 0.27 MPa. The micro-CT voxel intensity ranged 0–39 for void spaces in trabecular bone and 40–179 for cortical and trabecular bone tissue. The FEM computed strain in bone under implant loading was presented in Fig. 3 for a representative specimen #1. High strain appeared at the bone-implant contact locations and manifested into the supporting bone, including the buccal and lingual plates, which were not in direct contact with the implants. The strain concentration in the buccal plate was more substantial than that in the lingual plate. Specimen #2 exhibited a similar trend of strain distribution but with a lower magnitude than that in specimen #1.

The comparison of experimentally measured and FEM computed strain on the buccal and lingual bone surface is presented in Fig. 4. The strain concentration on the lingual bone (0.4%–0.5%) was less substantial than that on the buccal bone (~0.8%). The FEM computed strain distribution (Fig. 4b) was in good agreement with experimentally measured strain (Fig. 4a), in terms of the magnitude of strain. High strain started from the buccal crest in the experiment results (Fig. 4a), but it appeared at relatively lower locations in the FEM results (Fig. 4b). The relative differences between experimental measured and FEM calculated average strain in ROIs ranged from 4% to 22% (Fig. 5), with error bars representing one standard deviation. In both experimental results and simulation results, the buccal strain was higher than the lingual strain for both specimens. The average strain in specimen #1 (0.25%–0.50%) were generally higher than that in specimen #2 (0.13%–0.25%).

3.2. Effects of implant buccal distance

The FEM calculated strain distribution with different implant positions is presented in Fig. 6 for specimen #1. For all different positions, the strain concentration was more substantial on the buccal bone surface than that on the lingual bone surface. On the buccal bone surfaces, the size of high strain concentration area decreased with increasing relative buccal distance. On the lingual bone surfaces, the strain concentration was most substantial when the relative buccal bone distance was 48.2%, then it reduced when the implant was placed more towards lingual and buccal directions.
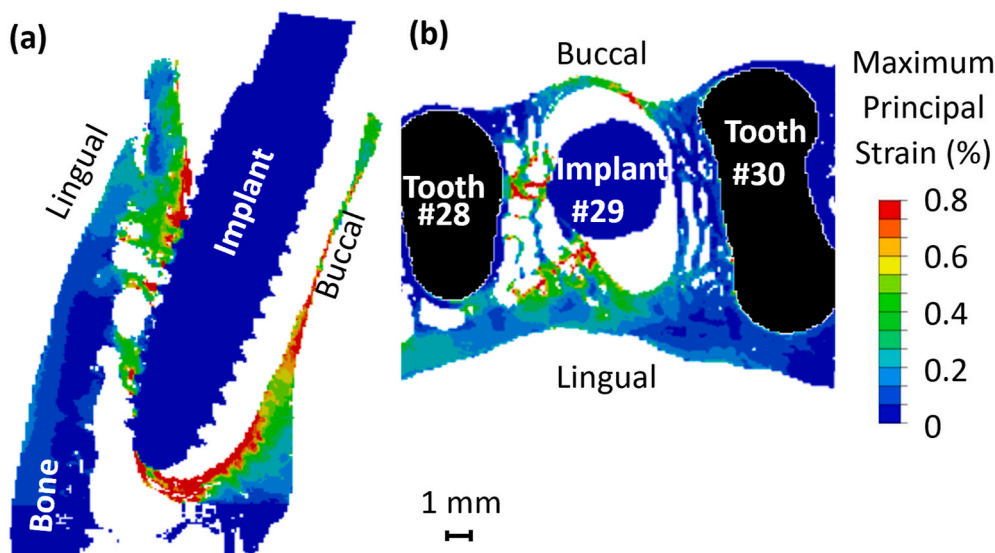

Fig. 3. Maximum principal strain distribution inside alveolar bone on (a) the buccolingual section and (b) the transverse sections for implant specimen #1 computed by FEM.
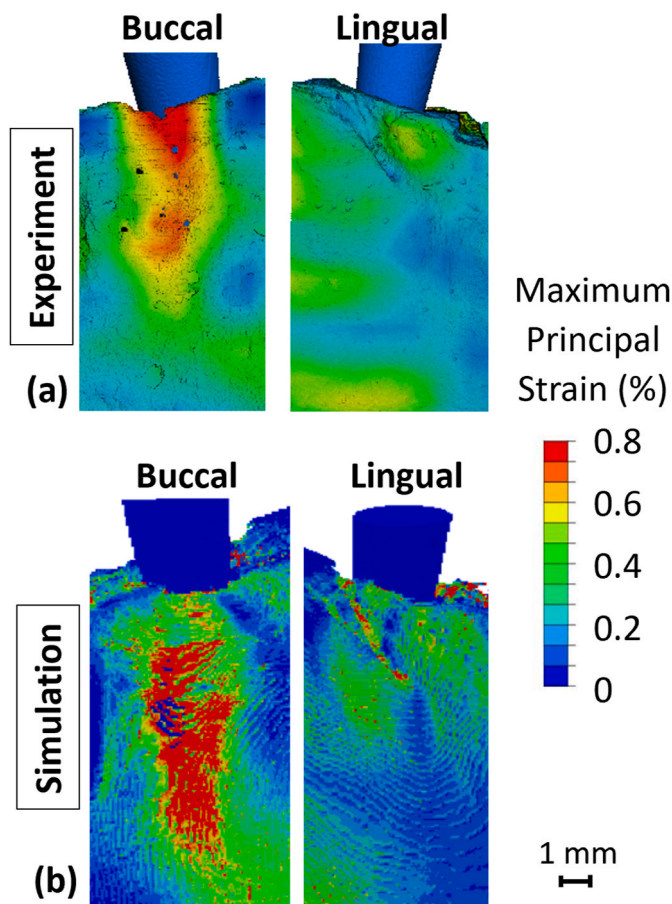
Fig. 4. Comparison of (a) experimentally measured and (b) FEM computed maximum principal strain distribution on the buccal and lingual bone surfaces around the implant for specimen #1.

The average strains in the fixed ROIs with different implant positions are presented in Fig. 7, with error bars representing one standard deviation. The average strain in buccal ROI decreased with increasing implant buccal distance in both specimens (Fig. 7). The average strain in lingual ROI was the highest for 48.2% buccal distance for both specimens. The average strain in buccal ROI was higher than that in the lingual ROI, for all implant positions and for both specimens. For each implant position, strain in specimen #1 (Fig. 7a) was higher than that in specimen #2 (Fig. 7b). Generally, strain in bone decreased with

increasing bone-implant contact area.

4. Discussion

4.1. Buccal bone strain

The results of this study provide insights to the outcomes of the immediate implant treatment. Buccal bone resorption is a risk for immediately placed implants (Chen and Buser, 2009, 2014; Kan et al., 2010). The results show that high strain appeared at bone-implant contact regions under implant loading, as expected (Fig. 3). High strain was also exhibited in buccal and lingual bone plates although these regions were not directly in contact with implants (Figs. 3 and 4). The alveolar sockets were expanded when the implants were loaded and it resulted in tensile strain in buccal and lingual bones. The strain in the buccal bone is higher than that in the lingual bone, because the buccal bone is thinner and less stiff than the lingual bone (Fig. 2). Our prior experimental and computational works have revealed similar strain distribution patterns (Du et al., 2015; Mao et al., 2019; Zhou et al., 2020).

The magnitude of strain in the buccal plate is related to its thickness. Stain in the buccal plate in specimen #1 was higher than that in specimen #2, when the buccal plate in specimen #1 was thinner than that in specimen #2. In our prior experiments, it has been shown that the strain in the buccal plate linearly increased with decreasing buccal plate thickness (Zhou et al., 2020). The strain concentration in buccal bone could be a contributing factor for the bone loss in this region. Using a combination of clinical investigation and finite element analysis, Li et al. have shown that the thickness of buccal plate played an important role in the mechanical stimuli, which consequentially determined the bone remodeling process (Yoda et al., 2017).

4.2. Effects of buccal distance of implant

The results of this study show that the mechanical stimuli in the buccal bone can be altered by changing the position of implants. The computed strain in the buccal bone decreased with increasing relative implant buccal distance (Figs. 6 and 7). The strain in lingual bone also deceased when the implant was moved from the center of the alveolar socket (48.2% relative buccal distance) (Fig. 7). In this study, it was difficult to see the occlusion relationship (contact between maxillary and mandibular teeth), since only mandibles were obtained. When determining implant position clinically, occlusion relationship must be considered along with other factors including conditions of alveolar bone, patient age and conditions of remaining teeth (Garg, 2007).

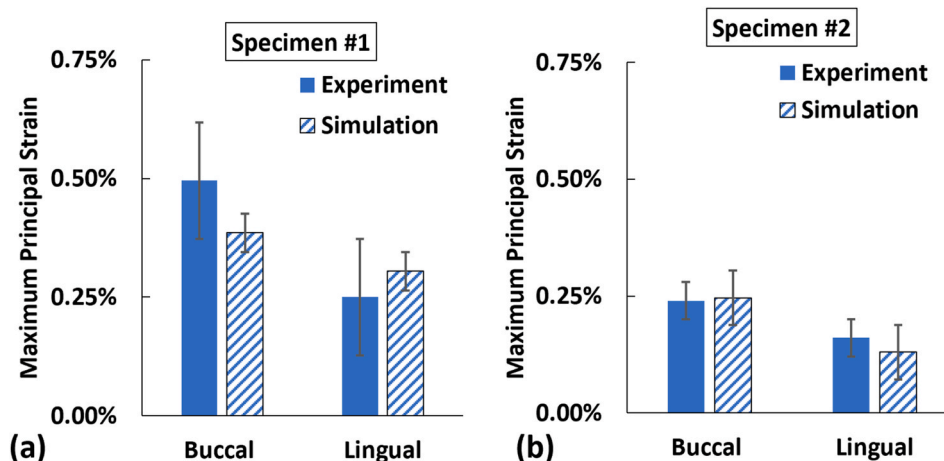The differences in mechanical stimuli may lead to different bone

Fig. 5. Comparison of experimentally measured strain and FEM computed strain in the buccal and lingual ROIs for (a) specimen #1 and (b) specimen #2.
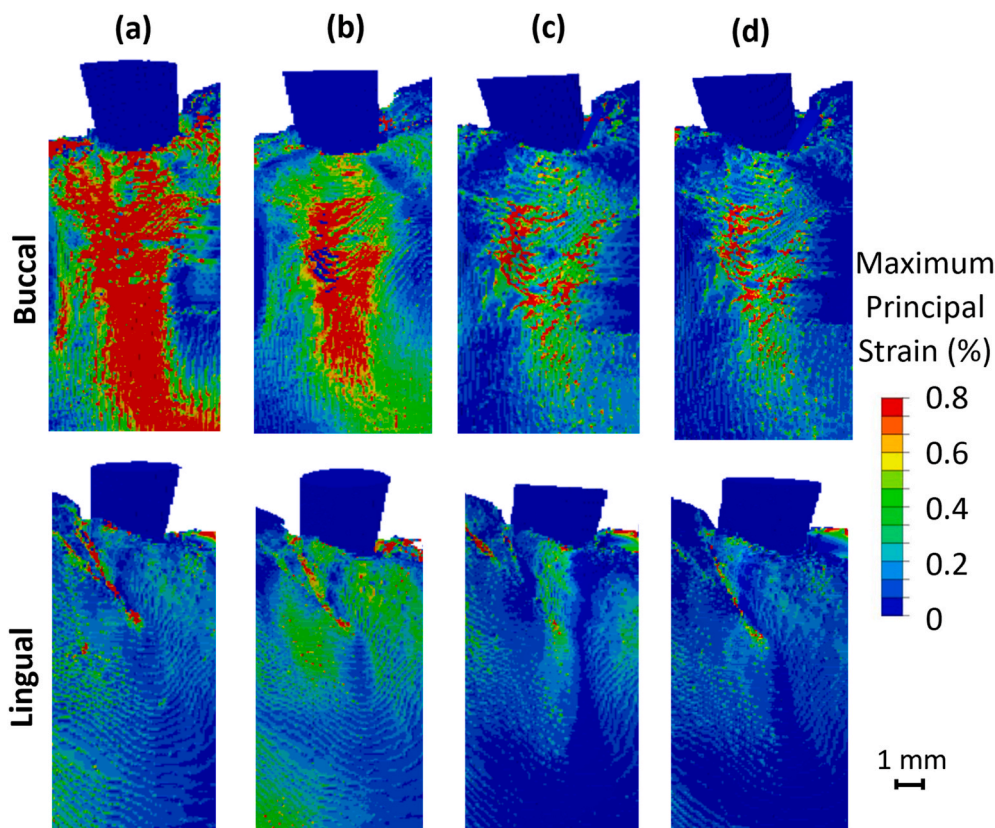
Fig. 6. Comparison of maximum principal strain on the buccal and lingual bone surfaces for specimen #1 with different implant positions predicted by FEM. The relative implant buccal distance was (a) 33.8% (b) 48.2% (c) 58.2% and (d) 73.5%, respectively. Implant position in (b) was at the same as that in the experiment.
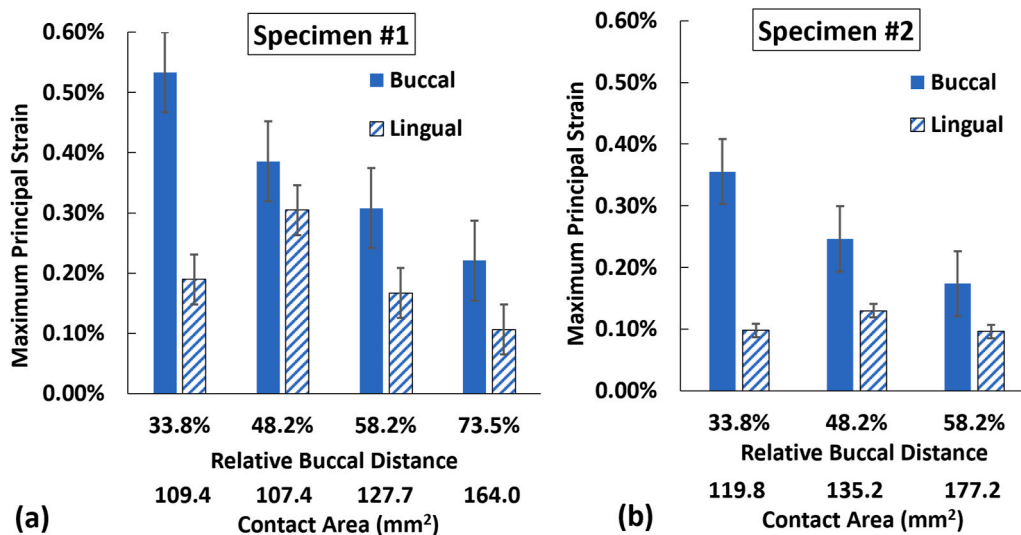

Fig. 7. Average maximum principal strain in the buccal and lingual ROIs predicted by FEM with different implant positions.

remodeling processes, which can result in different bone morphology. A clinical study by Chen et al. showed that buccal crest recession with lingually positioned implants was significantly lower than that with buccally positioned implants (Chen et al., 2007). Using an animal model, Pluemsakunthai et al. have shown that after immediate implant placement, among several groups with different buccal distances, when implant was placed furthest away from the buccal plate, the group had the highest buccal bone volume, the highest buccal bone/soft tissue thickness, and the lowest bone resorption (Pluemsakunthai et al., 2015).

4.3. Strain calculation

Among multiple strain components, maximum principal strain was chosen to be presented and discussed, because it was the characteristic strain under implant loading. The minimum principal strain under implant loading was also calculated. In general, its magnitude was much lower than the magnitude of maximum principal strain. This finding is consistent with the results in our prior computational work (Mao et al., 2019) and experimental work (Zhou et al., 2020). Moreover, in our prior

experiments, the median principal strain, minimum principal strain, and effective strain under implant loading were also measured (Zhou et al., 2020). No statistically significant correlation was found between these strain components and morphological factors, including buccal plate thickness (Zhou et al., 2020).

The average strain in the ROIs was reported, instead of the highest elemental strain. Because the highest elemental strain computed by FEM was dependent on the mesh for the trabecular bone microstructures and may not be at the same location in different models (Korabi et al., 2017). However, the characteristic high strain in buccal plate appeared in all models (Fig. 6).

In the experiments, digital volume correlation calculated the displacement for each block of voxels in the micro-CT image. Hence, the experimentally measured strain was the nominal strain for the blocks. In the simulation results, the average strain for all elements in each ROI, including the elements representing void spaces among trabecular bone, was calculated. Therefore, the computed strain was also the nominal strain for the ROI, which was consistent with the experimental results.

4.4. Model accuracy, limitations, and future works

There are several limitations associated with voxel-based finite element models for trabecular bone. In the models containing trabecular microstructures, the mesh often contained disconnected elements, that had insufficient constraints and usually resulted in zero-pivot warnings or numerical singularities (Ulrich et al., 1998). The techniques to improve mesh connectivity include tetrahedron elements (Müller and Rüegsegger, 1995; Ulrich et al., 1998), mass-compensated meshing (Ulrich et al., 1998), bone volume fraction based modulus (Mao et al., 2019). These processes still require image segmentation for individual trabeculae, which can be time-consuming and arbitrary.

In other image-based models without explicit trabecular microstructures, the elastic modulus of bone was assigned according to the local CT number or Hounsfield unit from the CT images (Keyak et al., 1990; Keyak and Skinner, 1992; Taddei et al., 2007). However, when metal implants were placed, beam hardening artifacts interfered with the CT number of bone and may even result in distorted images.

The FEM models in this work had several advantages compared with the above-mentioned methods. The elastic moduli of bone elements, including the void spaces in trabecular bone, were assigned based on the intensity value in the micro-CT images of bone-teeth structures before implant placement, which have no obvious beam hardening artifacts. There was no need to segment the individual trabeculae in micro-CT images, therefore it is less time-consuming and less arbitrary than those modeling the bone microstructures. There were no disconnected regions in the models, hence no zero-pivot warnings or numerical singularities. The elastic modulus for bone elements ranged from 0 to 432 MPa for void spaces in trabecular bone and up to 8.65 GPa for cortical bone and trabecular bone tissue, which is consistent with prior studies (Wirth et al., 2010).

Convergence study was performed with different element sizes in the models. The results indicated that the accuracy of the models could have been improved by further reducing the element size. However, the total number of elements/nodes in the models have reached the limitation of our computation capability.

The discrepancies between the experiment and FEM results can be attributed to the above-mentioned limitations of the models. Besides, many uncertainty factors contribute to the dispersion of the estimated mechanical properties of bone, such as the anisotropic tissue modulus (Basaruddin et al., 2015). The bone-implant interfaces may be also overly constrained in the FEM models. Micro-CT image artifacts could also cause inaccuracies in the experiment and FEM results.

Besides the implant position, the mechanics of bone-implant and the bone remodeling processes can also be influenced by other factors, such as the geometry of the implants, bone-implant interface properties, bone grafting procedure, the biology in osseointegration, and the microbiological factors. These are all possible directions for future work.

5. Conclusions

This paper presents the results of micro-CT based finite element analysis on bone-implant mechanics. The computed results show that high strain appeared at the buccal and lingual bone plates. The average strain in the buccal and lingual ROIs was in good agreement with those experimentally measured using mechanical testing coupled with micro-CT and digital volume correlation. The results also show that the mechanical stimuli in the buccal and lingual plates can be changed by altering the position of implants. Strain in buccal bone decreased when the implant was virtually placed in the models away from the buccal bone. The strain in lingual bone also deceased when the implant was virtually moved in the model away from the center of the alveolar socket. The results indicate that the distance from the implant to the buccal plate can affect the mechanical stimuli in bone, which may subsequently affect the bone remodeling process and bone resorption.

Author contributions

Kangning Su: Software, Validation, Formal analysis, Writing – original draft. Yuxiao Zhou: Investigation, Writing – review & editing. Mehran Hossaini-Zadeh: Investigation, Resources, Writing – review & editing. Jing Du: Conceptualization, Writing – review & editing, Supervision, Project administration, Funding acquisition.

Declaration of competing interest

The authors declare that they have no known competing financial interests or personal relationships that could have appeared to influence the work reported in this paper.

Acknowledgment

References

Basaruddin, K.S., Takano, N., Nakano, T., 2015. Stochastic multi-scale prediction on the apparent elastic moduli of trabecular bone considering uncertainties of biological apatite (BAp) crystallite orientation and image-based modelling. Comput. Methods Biomech. Biomed. Eng. 18, 162–174. https://doi.org/10.1080/10255842.2013.785537.

Brizuela-Velasco, A., Pérez-Pevida, E., Jiménez-Garrudo, A., Gil-Mur, F.J., Manero, J.M., Punset-Fuste, M., Chávarri-Prado, D., Diéguez-Pereira, M., Monticelli, F., 2017. Mechanical characterisation and biomechanical and biological behaviours of Ti-Zr binary-alloy dental implants. BioMed Res. Int. 1–10. https://doi.org/10.1155/2017/2785863, 2017.

Brunski, J.B., 1992. Biomechanical factors affecting the bone-dental implant interface. Clin. Mater. 10, 153–201. https://doi.org/10.1016/0267-6605(92)90049-Y.

Chen, S.T., Buser, D., 2014. Esthetic outcomes following immediate and early implant placement in the anterior maxilla–a systematic review. Int. J. Oral Maxillofac. Implants 29 (Suppl. l), 186–215. https://doi.org/10.11607/jomi.2014suppl.g3.3.

Chen, S.T., Buser, D., 2009. Clinical and esthetic outcomes of implants placed in postextraction sites. Int. J. Oral Maxillofac. Implants 24 (Suppl. l), 186–217.

Chen, S.T., Darby, I.B., Reynolds, E.C., 2007. A prospective clinical study of non-submerged immediate implants: clinical outcomes and esthetic results. Clin. Oral Implants Res. 18, 552–562. https://doi.org/10.1111/j.1600-0501.2007.01388.x.

Du, J., Lee, J.H., Jang, A.T., Gu, A., Hossaini-Zadeh, M., Prevost, R., Curtis, D.A., Ho, S. P., 2015. Biomechanics and strain mapping in bone as related to immediately-loaded dental implants. J. Biomech. 48, 3486–3494. https://doi.org/10.1016/j.jbiomech.2015.05.014.

Garg, A.K., 2007. Analyzing dental occlusion for implants: tekscan's TScan III. Dent. Implant. Update 18, 65–70.

Kan, J.Y.K., Rungcharassaeng, K., Lozada, J.L., Zimmerman, G., Kan, Joseph Y.K., Rungcharassaeng, Kitichai, Lozada, Jaime L., Zimmerman, G., Kan, J.Y.K., Rungcharassaeng, K., Lozada, J.L., Zimmerman, G., 2010. Facial gingival tissue stability following immediate placement and provisionalization of maxillary anterior single implants: a 2- to 8-year follow-up. Int. J. Oral Maxillofac. Implants 26, 179–187.

Keyak, J.H., Meagher, J.M., Skinner, H.B., Mote, C.D., 1990. Automated three-dimensional finite element modelling of bone: a new method. J. Biomed. Eng. 12, 389–397. https://doi.org/10.1016/0141-5425(90)90022-F.

Keyak, J.H., Skinner, H.B., 1992. Three-dimensional finite element modelling of bone: effects of element size. J. Biomed. Eng. 14, 483–489. https://doi.org/10.1016/0141-5425(92)90100-Y.

Korabi, R., Shemtov-Yona, K., Dorogoy, A., Rittel, D., 2017. The failure envelope concept applied to the bone-dental implant system. Sci. Rep. 7, 2051. https://doi.org/10.1038/s41598-017-02282-2.

Leucht, P., Kim, J., Wazen, R., Currey, J.A., Nanci, A., Brunski, J.B., Helms, J.A., 2007. Effect of mechanical stimuli on skeletal regeneration around implants. Bone 40, 919–930. https://doi.org/10.1016/j.bone.2006.10.027.

Mao, Q., Su, K., Zhou, Y., Hossaini-Zadeh, M., Lewis, G.S., Du, J., 2019. Voxel-based micro-finite element analysis of dental implants in a human cadaveric mandible: tissue modulus assignment and sensitivity analyses. J. Mech. Behav. Biomed. Mater. 94, 229–237. https://doi.org/10.1016/j.jmbbm.2019.03.008.

Müller, R., Rüegsegger, P., 1995. Three-dimensional finite element modelling of non-invasively assessed trabecular bone structures. Med. Eng. Phys. 17, 126–133. https://doi.org/10.1016/1350-4533(95)91884-J.

Pluemsakunthai, W., Le, B., Kasugai, S., 2015. Effect of buccal gap distance on alveolar ridge alteration after immediate implant placement: a microcomputed tomographic and morphometric analysis in dogs. Implant Dent. 24, 70–76. https://doi.org/10.1097/ID.0000000000000194.

Soboyejo, W., 2003. Mechanical Properties of Engineered Materials. New York. CRC, New York.

Taddei, F., Schileo, E., Helgason, B., Cristofolini, L., Viceconti, M., 2007. The material mapping strategy influences the accuracy of CT-based finite element models of bones: an evaluation against experimental measurements. Med. Eng. Phys. 29, 973–979. https://doi.org/10.1016/j.medengphy.2006.10.014.

Ulrich, D., Van Rietbergen, B., Weinans, H., Rüegsegger, P., 1998. Finite element analysis of trabecular bone structure: a comparison of image-based meshing techniques. J. Biomech. 31, 1187–1192. https://doi.org/10.1016/S0021-9290(98)00118-3.

Wazen, R.M., Currey, J.A., Guo, H., Brunski, J.B., Helms, J.A., Nanci, A., 2013. Micromotion-induced strain fields influence early stages of repair at bone–implant interfaces. Acta Biomater. 9, 6663–6674. https://doi.org/10.1016/j.actbio.2013.01.014.

Wirth, A.J., Mueller, T.L., Vereecken, W., Flaig, C., Arbenz, P., Müller, R., van Lenthe, G. H., 2010. Mechanical competence of bone-implant systems can accurately be determined by image-based micro-finite element analyses. Arch. Appl. Mech. 80, 513–525. https://doi.org/10.1007/s00419-009-0387-x.

Yoda, N., Zheng, K., Chen, J., Li, W., Swain, M., Sasaki, K., Li, Q., 2017. Bone morphological effects on post-implantation remodeling of maxillary anterior buccal bone: a clinical and biomechanical study. J. Prosthodont. Res. 61, 393–402. https://doi.org/10.1016/j.jpor.2016.12.010.

Zhou, Y., Gong, C., Hossaini-Zadeh, M., Du, J., 2020. 3D full-field strain in bone-implant and bone-tooth constructs and their morphological influential factors. J. Mech. Behav. Biomed. Mater. 110, 103858 https://doi.org/10.1016/j.jmbbm.2020.103858.